SENSOR CORRECTION AND RADIOMETRIC CALIBRATION OF A 6-BAND MULTISPECTRAL IMAGING SENSOR FOR UAV REMOTE SENSING

Joshua Kelcey and Arko Lucieer

School of Geography and Environmental Studies
University of Tasmania
Private Bag 76, Hobart, Tasmania, 7001, Australia
josh.kelcey@utas.edu.au, arko.lucieer@utas.edu.au

KEY WORDS: Correction, Processing, High resolution, Radiometric, Sensor

ABSTRACT:

The increased availability of unmanned aerial vehicles (UAVs) has resulted in their frequent adoption for a growing range of remote sensing tasks which include precision agriculture, vegetation surveying and fine-scale topographic mapping. The development and utilisation of UAV platforms requires broad technical skills covering the three major facets of remote sensing: data acquisition, data post-processing, and image analysis. In this study, UAV image data acquired by a miniature 6-band multispectral imaging sensor was corrected and calibrated using practical image-based data post-processing techniques. Data correction techniques included dark offset subtraction to reduce sensor noise, flat-field derived per-pixel look-up-tables to correct vignetting, and implementation of the Brown-Conrady model to correct lens distortion. Radiometric calibration was conducted with an image-based empirical line model using pseudo-invariant features (PIFs). Sensor corrections and radiometric calibration improve the quality of the data, aiding quantitative analysis and generating consistency with other calibrated datasets.

1 INTRODUCTION

Unmanned aerial vehicles occupy a previously unfilled niche through their capability to generate ultra high spatial resolution image data at highly flexible temporal scales (Dunford et al., 2009). UAV imagery has value as a sole source of data, or used to fill gaps in scale between fine scale field samples and coarser scale aerial photography or satellite imagery. As a remote sensing platform, UAVs offer the scientific community an unprecedented level of accessibility and flexibility in data generation. The growing availability of small, low cost, components have provided research groups with the opportunity to tailor a remote sensing platform to fit their own specific research niches.

UAV development and operation require a range of technical skills covering platform development, image data post-processing and image analysis techniques. Post-processing techniques improve data quality and generates consistency with other calibrated image sets. Raw image data is strongly influenced and modified by a number of sources which include environmental conditions and sensor characteristics (M. Smith, 1999, Mahiny and Turner, 2007). These modifications place severe limitations upon the quality and validity of further quantitative analysis. Image data post-processing encompasses the techniques used to consistently extract surface reflectance information from raw data. Post-processing can be broadly divided into two main phases: sensor correction and radiometric calibration.

1.1 Sensor Correction

Sensor correction is the first phase of image data post-processing and encompasses the techniques used to reduce data modifications generated by the sensor. Sensor-based modifications may arise during the collection, processing, and transmission of data by the system (Al-amri et al., 2010). These modifications include processes that either introduce additional measurements, obscure measurements or alter the spatial properties of incoming light.

Sensor-based data modifications include the effects of noise, vignetting and lens distortion. Noise is defined as any additive, unwanted measurement that is generated by the sensor independently of incoming light (Mansouri et al., 2005). Vignetting is a radial falloff in illumination strength caused primarily by increased occlusion of the detector plane by the sensor (Goldman, 2010, Kim and Pollefeys, 2008). Vignetting results in a radial shadowing effect towards the image periphery. Lens distortion is generated by an uneven magnification across a lens surface and can be further degraded by a misalignment between lens and detector plane (Hugemann, 2010, Wang et al., 2006). Lens distortion results in a radial displacement of a measurements true position.

1.2 Radiometric Calibration

Radiometric calibration is the second phase of image data post-processing and encompasses the techniques used to reduce the effects of relative environmental variables and extract absolute reflectance measurements from the data. Remotely sensed measurements are highly influenced by the environmental conditions present at the time of data generation. Environmental variables include atmospheric composition, surface conditions and temporal changes in light level (Hadjimitsis et al., 2004). Radiometric calibration is essential for generating consistency in remotely sensed imagery acquired under a wide variety of environmental conditions (Cooley et al., 2002).

The primary focus of this study is to provide a practical, primarily image-based, data post-processing workflow applicable to UAV remote sensing. The study provides a linear workflow of sensor correction and radiometric calibration steps for a low cost, consumer grade multispectral sensor. Steps are illustrated with a practical worked example.

2 METHODS

2.1 UAV and Sensor

The UAV constructed for this study consisted of a MikroKopter Oktokopter[1] frame (see Fig.1) mounted with the miniature cam-

[1] http://www.mikrokopter.de

Figure 1: MikroKopter Oktokopter with mounted mini-MCA Multispectral Sensor (Photo: Darren Turner)

era array (mini-MCA). The mini-MCA is a small, low-cost six-band multispectral sensor manufactured by Tetracam inc[2]. The mini-MCA system consists of an array of six individual channels. Each mini-MCA channel is equipped with a CMOS sensor and a fixed objective lens and aperture length. Factory provided standards illustrate the monochromatic efficiency of the CMOS chip over a range of 400 to 1120 nm. Each channel is additionally fitted with mountings for an interchangeable band-pass filter, allowing users to define the spectral band configuration of the system. Image band data is collected at a image resolution of 1280x1024 at a dynamic range of either 8 or 10 bits.

2.2 Study Site and Data Collection

The Ralphs Bay area in Tasmania, Australia is a stretch of sheltered coastline undergoing urban encroachment and commercial development. The bay provides limited areas of shelter from strong scouring ocean tides, allowing for the establishment of salt marsh. Salt marsh is a vegetation type that occurs primarily within riparian or coastal areas and is dominated by species that exhibit strong tolerance for water logging and/or saline conditions (Emery et al., 2001). The strong water/saline gradients exhibited along shorelines typically results in a strong zonation in the distribution of salt marsh species (Pennings et al., 2005, Emery et al., 2001). The topographic flatness and relatively simple distribution of species within salt marsh provides an uncomplicated environment for UAV research and development.

Figure 2: Location of Salt Marsh Study Site at Ralphs Bay, Tasmania, Australia (Map Source: GoogleEarth)

An area of Ralphs Bay salt marsh was selected to serve as a test site. UAV salt marsh missions were conducted at heights of 50 m and 100 m at an exposure of 2,000 and 4,000. Multispectral imagery was generated by the mini-MCA with a bandpass filter configuration of in order of channel: 700, 490, 530, 570, 670, 750 nm. Over 50 field samples were acquired from across the study site. Each field sample consisted of a GPS point, a geolocated true colour digital photograph and an at-surface spectral reflectance measurement. GPS points were acquired using a Leica GPS1200 RTK system. Geolocated photographs were taken using a Canon 50D. Spectral measurements were acquired using the ASD HandHeld 2 Portable Spectrometer. A single mini-MCA salt marsh image acquired at 100 m at an exposure of 4,000 was selected to demonstrate the data post-processing workflow.

2.3 Image Data Processing

Raw mini-MCA image data was converted to 10 bit digital number (DN) imagery using IDL script within the ENVI[3] spatial software package. Sensor correction and radiometric calibration processing and application steps were also implemented through IDL script within the ENVI environment. Image band stacking and coregistration was implemented through ENVI.

2.4 Sensor Correction

2.4.1 Noise Reduction Sensor noise is additional, additive measurements that are generated by a sensor independently to an incoming signal (Mansouri et al., 2005). Sources of sensor noise include electrical interference, variable environmental conditions and variation across the detector plane erroneously introduced during manufacture. Raw data measurements are the sum of an incoming signal component and a noise component. The smaller the ratio of the signal component to the noise component becomes, the greater the true data measurement is obscured.

Noise correction requires an estimation of the noise component within the data. Noise, however, exhibits random temporal properties within its distribution (Mansouri et al., 2005). The exact proportion of sensor noise within image data at any given time, therefore, cannot be precisely calculated. Instead techniques focus upon estimating and reducing sensor noise.

Dark offset subtraction is an image based approach for sensor noise reduction (Mansouri et al., 2005, Mullikin, 1994). The technique exploits the independence in the origin of sensor noise from the incoming signal component. Dark offset imagery is imagery that is generated in the absence of any incoming light. This technique effectively removes the incoming signal component from the measured data, thus providing a sample of the per-pixel sensor noise component. Through repetition, the average per-pixel sensor noise may be estimated. The per-pixel subtraction of this average dark offset from other imagery provides a method of noise reduction. The per-pixel standard deviation of dark offset imagery provides an estimation of the average per-pixel sensor noise remaining within imagery following dark offset subtraction.

2.4.2 Dark Offset Image Generation Methodology Mini-MCA dark offset imagery was generated within a dark room. The mini-MCA was further enveloped by a Gore-Tex hood to provide an additional barrier to incoming light. Dark offset imagery was generated for each of the six mini-MCA channels. The exposure was set to 4,000 to match the UAV salt marsh test image. A total of 125 sample dark offset images were generated for each channel from which the per-pixel average and standard deviation were calculated. Dark offset subtraction was applied to the corresponding UAV salt marsh test image bands.

[2]http://www.tetracam.com

[3]http://www.ittvis.com

2.4.3 Vignetting Correction Vignetting is a radially dependent falloff in illumination strength. It is typically caused by sensor components (e.g. barrel) occluding light from the detector plane at wide angles (Goldman, 2010). Increased angles of incoming light result in stronger occlusion. This increasing occlusion manifests as a radial shadowing effect that increases towards the image periphery.

Flat field derived correction factor look-up-tables (LUT) represent an image based approach to vignetting correction. Flat fields are surfaces that exhibit uniform, spectrally homogeneous Lambertian properties (Mansouri et al., 2005). Generated imagery of flat field surfaces, under the effects of vignetting, exhibit characteristic radial deviation away from a homogeneous condition. A quantitative assessment of this deviation allows for the per-pixel modelling of the vignetting illumination falloff. The method rests upon the assumption that the brightest pixel within the flat field image exhibits the correct flat field measurement. Correction factors are then calculated for the remaining pixels to restore their value to the brightest, correct flat field measurement. Imagery modified by vignetting may be corrected through a per-pixel multiplication with this flat field derived correction factor imagery (Mansouri et al., 2005, Yu, 2004).

2.4.4 Vignetting Correction Factor LUT Methodology A white artist's canvas was utilised as a flat field surface. Mini-MCA flat field imagery for each of the six individual channels was generated from the flat field. To improve noise reduction, 125 sample flat field images were generated for each sensor. The average of these 125 sample images was calculated to improve correspondence between the averaged noise component within the dark offset imagery and flat field imagery. Dark offset subtraction was performed upon each averaged flat field image. Sensor dependent vignetting correction factor LUTs were calculated from each averaged flat field. Vignetting correction was applied to the corresponding UAV salt marsh test image band.

2.5 Lens Distortion

Lens distortion is characterised by a radial shift in a measurements true position. It is primarily generated by non-uniform magnification across a lens surface and may be further influenced by the misalignment between the lens and detector plane. Non-uniform magnification results in a radial shifting of measurements. This is typically a shift away from the image centre (barrel distortion) or towards the image centre (pincushion distortion). Misalignment between lens and detector plane results in a planar shift in the perspective of an image (Wang et al., 2009, Hugemann, 2010, Prescott, 1997).

The Brown-Conrady lens distortion model is capable of correcting the effects of both non-uniform magnification and lens/detector plane misalignment. The model, however, requires the calculation of sensor specific intrinsic and extrinsic coefficients. A common approach for the calculation of these coefficients is through the use of calibration panels. A calibration panel is typically a planar grid of known geometric properties. Imagery is generated of the calibration panel from multiple angles. Sensor specific intrinsic and extrinsic coefficients are calculated based upon point correspondence between the known geometric properties of the calibration panel and the distorted geometric properties exhibited within imagery (Wang et al., 2006, Hugemann, 2010).

2.5.1 Lens Distortion Correction Methodology Mini-MCA imagery of a calibration panel was generated for each individual channel from multiple angles. Corresponding dark offset subtraction and vignetting correction was applied to the calibration panel imagery. For each mini-MCA channel, the intrinsic and extrinsic coefficients were calculated from the calibration panel imagery using the Agisoft Lens[4] software package. The Brown-Conrady lens distortion model was implemented using the extracted coefficients for each separate channel. Lens distortion was corrected in the UAV salt marsh test imagery for each corresponding band.

2.6 Radiometric Calibration

2.6.1 Empirical Line Regression The empirical line method is an image-based empirical approach to radiometric correction. The technique is built upon the assumption that an empirical relationship exists between the collected sensor DN measurements and the at-surface reflectance (M. Smith, 1999). Calculation of this empirical relationship allows the conversion of the collected data into at-surface reflectance measurements. This empirical relationship is commonly extracted through the use of targets of measured at-surface reflectance properties known as pseudo-invariant features (PIFs) (Moran, 2001).

The suitability of PIFs is based upon several attributes. A PIF is required to be spectrally homogeneous with Lambertian reflectance properties and spectrally invariant with environmental conditions. The empirical line method requires that measurements are taken for at least two PIFs, one light and one dark. The relationship between the at-sensor PIF DN measurements recorded within the imagery and the at-surface reflectance acquired from field measurements is analysed, and a linear relationship for each band derived (Karpouzli and Malthus, 2003, M. Smith, 1999). Imagery is then converted to at-surface reflectance through the use of these linear equations.

2.6.2 Empirical Line Regression Methodology Three PIFs were constructed composing of a plywood wood backing with a white tyvac, an intermediate grey fabric and black fabric covers respectively. The PIFs were placed within the salt marsh study site prior to UAV flight. At-surface reflectance measurements from the PIFs were acquired using an ASD HandHeld 2 Portable Spectrometer. Linear relationships were calculated between the sensor corrected spectral bands generated by the mini-MCA and the corresponding at-surface reflectance measurements recorded by the spectrometer. Sensor measurements were converted into reflectance measurements by applying each linear equation to its corresponding UAV salt marsh test image band.

3 RESULTS

A six band multispectral UAV acquired salt marsh image was selected to serve as a test case for image based data post-processing (see Fig. 3).

3.1 Dark Offset Subtraction

Dark offset imagery was generated for each of the six mini-MCA channels at an exposure of 4,000. Figure 4 provides a comparison of the six channels reveals channel 4 to have the highest average noise (greater than 12 DN). Channel 6 records the lowest average noise (5 DN). An examination of the standard deviation reveals that the channel 4, despite recording the highest average noise, is also the most responsive to dark offset subtraction (average of 92% reduction in noise). Channels 5 and 6 record the worst response to dark offset subtraction (56% and 51% reductions respectively). The differing response of noise within each of the dark offset imagery reveals the channel dependence of noise measurements.

[4] http://www.agisoft.ru/products/lens

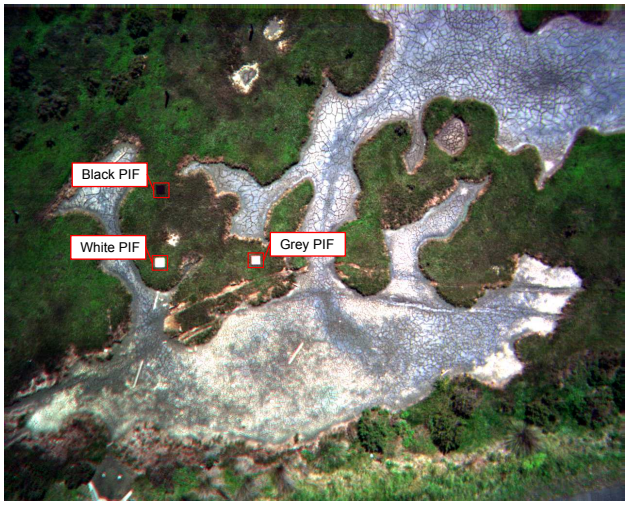

Figure 3: Uncorrected True Colour UAV Salt Marsh Test Image (Image Bands Coregistered)

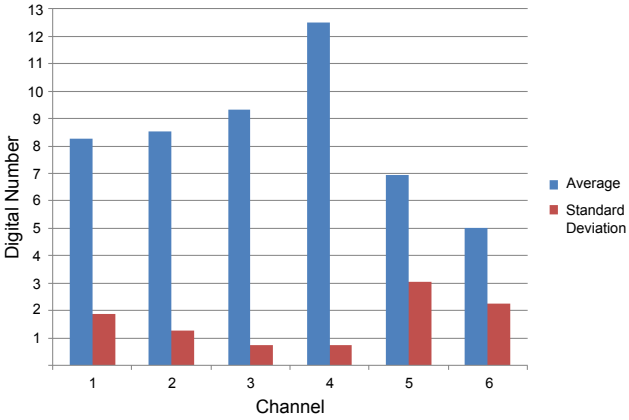

Figure 4: Per-Pixel Noise Average and Standard Deviation for each mini-MCA Channels (exposure: 4,000)

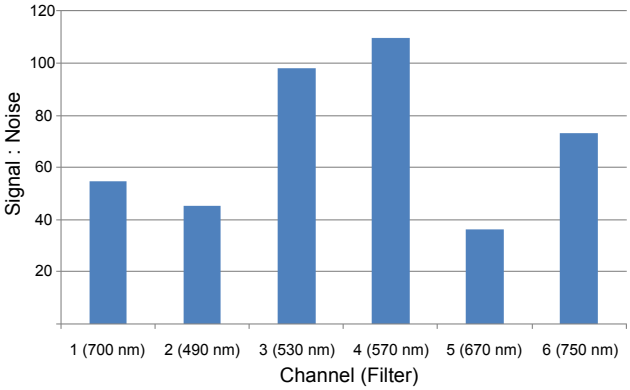

Figure 5: SNR of UAV Salt Marsh Test Image Bands

Signal-to-noise ratio was calculated as the ratio of the average image measurement post-dark offset subtraction to the standard deviation of the dark offset imagery. An assessment of SNR reveals channel 4 and 3 to have generated the highest quality of data. Both channel 4 and 3 are equipped with filters within the low monochromatic efficiency range of the mini-MCA. Conversely the high efficiency range of the channel 6 filter offsets the poor performance of dark offset subtraction. This demonstrates that data quality across the system may be balanced through the careful match of monochromatic efficiency with dark offset subtraction potential.

3.2 Vignetting

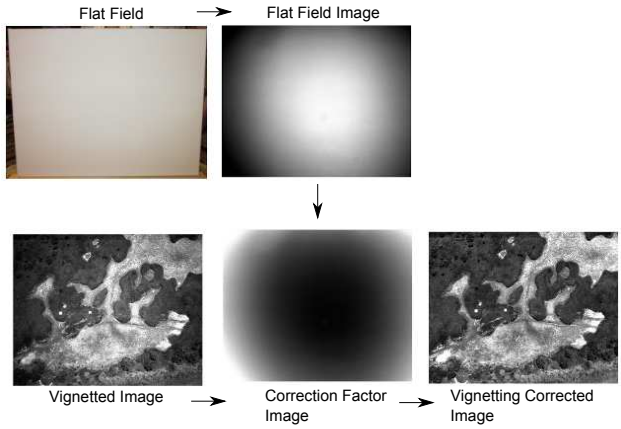

Figure 6: Illustration of the Generation of Flat Field derived Corrections Factor Images, and their application to imagery (Channel: 3)

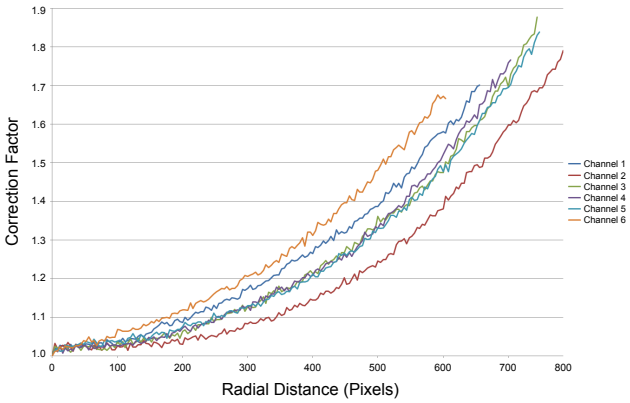

Figure 7: Rate of Correction Factor Change

Flat field imagery was generated for each of the six mini-MCA channels. Vignetting correction factor look-up-tables (LUT) were derived from each flat field. Vignetting in salt marsh UAV image bands was corrected through application of correction factor imagery (see Fig.6). LUTs recorded differences in the rate of radial illumination falloff (see Fig.7). The rate of vignetting illumination falloff was quickest within channel 6, and slowest within channel 2. These differences in falloff rate illustrate the channel dependence of vignetting correction factor LUTs.

3.3 Lens Distortion Correction

Imagery of a planar calibration panel was generated for each of the six mini-MCA channels. The intrinsic and extrinsic coefficients for each channel were calculated from these images using the AgiSoft Lens software package. The Brown-Conrady lens distortion model was implemented for each channel using the corresponding coefficients. All the mini-MCA channels exhibited barrel distortion. The rate of radial shift varied between channels (see Fig.8). Channels 4 and 6 exhibited the strongest distortion. Channel 2 exhibited the weakest distortion. The differing rates of radial shift between channels illustrates the channel dependence of lens distortion correction.

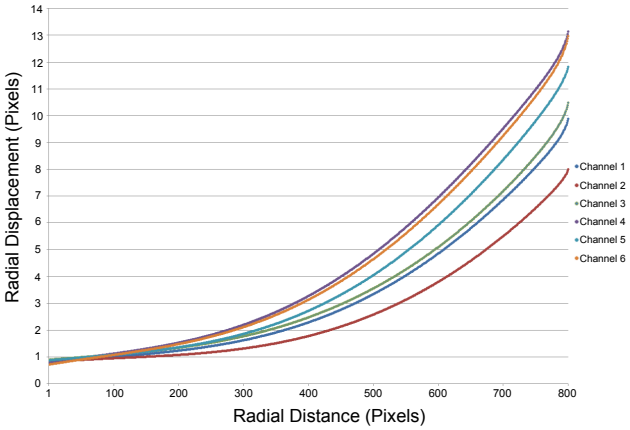

Figure 8: Rate of Lens Distortion Radial Shift

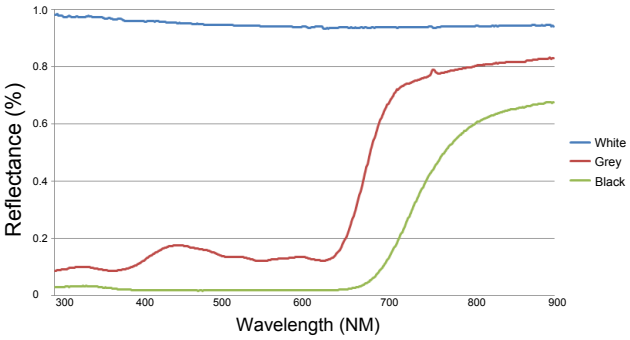

Figure 9: Spectral Response of Pseudo Invariant Features

3.4 Empirical Line Regression

The spectral response of the PIFs as measured by the spectrometer is illustrated in Figure 9. Both the grey and black PIf exhibit highly spectrally variant responses, clearly illustrating the unsuitability of cotton fabric as a PIF material. Field measurements of the PIF targets acquired within the field were regressed against the sensor corrected PIF DN measurements. Linear relationships were extracted and applied to the mini-MCA imagery to convert sensor DN values into at-surface reflectance measurements. Figure 10 provides an illustrative example of the calibration performance of the mini-MCA through a direct comparison of the spectral response of salt marsh landcover classes by the ASD spectrometer.

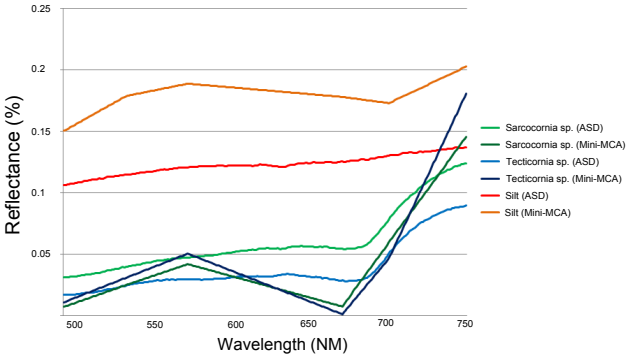

Figure 10: Illustrative Comparison of the Spectral Response of Salt Marsh landcover classes recorded by the ASD spectrometer and the calibrated mini-MCA.

Figure 11: Visual comparison of the improvements by the application of sensor corrections and radiometric calibration (Image Bands Coregistered).

3.5 Final Comparison

Figure 11 is a visual illustration of the improvements to the UAV salt marsh test imagery that both sensor corrections and radiometric calibration provide.

4 DISCUSSION

The science of remote sensing can be divided into three broad phases: image acquisition, data post-processing and image analysis. These three phases exhibit a circular dependence. Image acquisition is strongly influenced by the user's choice of analysis methods and goals. Data post-processing is dependent upon sensor settings and characteristics during image acquisition. The validity of image analysis is strongly influenced by the success of data post-processing techniques.

The availability of UAV platforms to smaller research group has allowed for all three phases of remote sensing to be carried out in-house. Research groups are therefore required to have a broader technical skillset to adequately address all three phases. This provides UAV research groups a significant advantage in the capacity to tailor all three interdependent phases to their specific research requirements.

Image data post-processing is an essential phase for both the improvement of data quality and for generating consistency with other datasets. Dark offset imagery, vignetting and lens distortion all exhibit channel dependent characteristics. Therefore, the implemented data post-processing techniques were strongly dependent upon settings and characteristics of the mini-MCA to derive the appropriate information required to successfully apply the corrections.

4.1 SNR Sensor Balance

The capacity for dark offset subtraction to reduce noise within the mini-MCA ranged in average per-pixel reduction of 54.9% (channel 6) to 94% (channel 4). The proportion of noise within the data, however, is only one factor within the overall SNR. The SNR is also dependent upon the proportion of signal within the data. A strong determinate of the signal strength for the mini-MCA is the monochromatic efficiency of the sensor. In order to balance SNR across the mini-MCA, it becomes important to identify the relative noise performance of individual channels. A balance in the SNR across the system may then be achieved by matching the noise performance of individual channels with an appropriate bandpass filters (i.e. low efficiency wavelengths with low noise channels, high efficiency with high noise).

4.2 Pseudo-Invariant Feature Selection

The selection of PIFs is central to the generation of an accurate Empirical line. Past studies to have utilised PIFs have included man-made or natural surfaces present within satellite or aerial imagery (Karpouzli and Malthus, 2003, M. Smith, 1999). Typically these features are required to cover large spatial extents to provide a pure surface spectral measurement within the captured imagery. The ultra high resolution of UAV imagery, however, have significantly reduced the required spatial extents of required targets enough that it has now become practical to construct them for use in the field. This flexibility has allowed researchers to incorporate materials with more suitable spectral properties. Studies continue in the search for suitable, spectrally homogeneous materials suitable for PIF targets.

5 CONCLUSION

The mini-MCA is a low-cost, lightweight 6-channel multispectral sensor suited to UAV remote sensing research. Primarily image-based data post-processing techniques were applied to UAV generated salt marsh imagery. Sensor corrections were implemented to improve data quality. Radiometric calibration was implemented to generate consistency with other datasets. The success of data post-processing techniques is dependent upon sensor characteristics. In order to maximise the effects of data post-processing of image data, it becomes necessary to modify image acquisition approaches to balance sensor characteristics.

Remote sensing can be broadly divided into three phases: image acquisition, data post-processing and image analysis. Remote sensing research groups exploring UAVs as a remote sensing platform require a broad skillset to accommodate all three phases. Remote sensing studies are dependent upon robust quantitative data. For UAV-based research, this will require the development of practical, improved techniques and developmental pathways that address the interplay between all three phases of remote sensing.

ACKNOWLEDGEMENTS

The authors would like to acknowledge the Winifred Violet Scott Trust and the Australian Antarctic Division for financially supporting this project. We thank Darren Turner for his technical input and UAV piloting skills in the field. Finally, we would like to thank Dr Jon Osborn for his advice on sensor correction.

REFERENCES

Al-amri, S. S., Kalyankar, N. V. and Khamitkar, S. D., 2010. A Comparative Study of Removal Noise from Remote Sensing Image. Journal of Computer Science 7(1), pp. 32–36.

Cooley, T., Anderson, G., Felde, G., Hoke, M., a.J. Ratkowski, Chetwynd, J., Gardner, J., Adler-Golden, S., Matthew, M., Berk, a., Bernstein, L., Acharya, P., Miller, D. and Lewis, P., 2002. FLAASH, a MODTRAN4-based atmospheric correction algorithm, its application and validation. IEEE International Geoscience and Remote Sensing Symposium 3(C), pp. 1414–1418.

Dunford, R., Michel, K., Gagnage, M., Piegay, H. and Tremelo, M. L., 2009. Potential and constraints of Unmanned Aerial Vehicle technology for the characterization of Mediterranean riparian forest. International Journal of Remote Sensing 30(19), pp. 4915–4935.

Emery, N. C., Ewanchuk, P. J. and Bertness, M. D., 2001. Competition and Salt-Marsh Plant Zonation: Stress Tolerators May Be Dominant Competitors. Ecology 82(9), pp. 2471–2485.

Goldman, D. B., 2010. Vignette and exposure calibration and compensation. IEEE transactions on pattern analysis and machine intelligence 32(12), pp. 2276–88.

Hadjimitsis, D. G., Clayton, C. R. I. and Hope, V. S., 2004. An assessment of the effectiveness of atmospheric correction algorithms through the remote sensing of some reservoirs. International Journal of Remote Sensing 25(18), pp. 3651–3674.

Hugemann, W., 2010. Correcting Lens Distortions in Digital Photographs.

Karpouzli, E. and Malthus, T., 2003. The empirical line method for the atmospheric correction of IKONOS imagery. International Journal of Remote Sensing 24(5), pp. 1143–1150.

Kim, S. J. and Pollefeys, M., 2008. Robust radiometric calibration and vignetting correction. IEEE transactions on pattern analysis and machine intelligence 30(4), pp. 562–76.

M. Smith, Edward J. Milton, G., 1999. The use of the empirical line method to calibrate remotely sensed data to reflectance. International Journal of Remote Sensing 20(13), pp. 2653–2662.

Mahiny, A. S. and Turner, B. J., 2007. A Comparison of Four Common Atmospheric Correction Methods. Photogrammetric Engineering & Remote Sensing 73(4), pp. 361–368.

Mansouri, A., Marzani, F. and Gouton, P., 2005. Development of a Protocol for CCD Calibration: Application to a Multispectral Imaging System. International Journal of Robotics and Automation.

Moran, M., 2001. A refined empirical line approach for reflectance factor retrieval from Landsat-5 TM and Landsat-7 ETM+. Remote Sensing of Environment 78(1-2), pp. 71–82.

Mullikin, J. C., 1994. Methods for CCD camera characterization. Proceedings of SPIE 2173, pp. 73–84.

Pennings, S. C., Grant, M.-B. and Bertness, M. D., 2005. Plant zonation in low-latitude salt marshes: disentangling the roles of flooding, salinity and competition. Journal of Ecology 93(1), pp. 159–167.

Prescott, B., 1997. Line-Based Correction of Radial Lens Distortion. Graphical Models and Image Processing 59(1), pp. 39–47.

Wang, A., Qiu, T. and Shao, L., 2009. A Simple Method of Radial Distortion Correction with Centre ofDistortion Estimation. Journal of Mathematical Imaging and Vision 35(3), pp. 165–172.

Wang, J., Shi, F., Zhang, J. and Liu, Y., 2006. A New Calibration Model and Method of Camera Lens Distortion. 2006 IEEE/RSJ International Conference on Intelligent Robots and Systems pp. 5713–5718.

Yu, W., 2004. Practical anti-vignetting methods for digital cameras. IEEE Transactions on Consumer Electronics 50(4), pp. 975–983.